Bulgarian Chemical Communications, Volume 58, Issue 2 (pp. 143-153) 2026 *DOI: 10.34049/bcc.58.2.5733*

Unveiling mechanisms of action of isoquinoline alkaloids from *Hylomecon japonica* as promising inhibitors of breast cancer through computational modelling

H. D. Nguyen*

Faculty of Biology, Thai Nguyen University of Education, 24124 Thai Nguyen, Vietnam

Received: November 26, 2025; Revised: March 03, 2026

Breast cancer remains the leading cancer diagnosis and cause of cancer-related mortality in women, accounting for approximately 25% of new female cases and around 670,000 deaths globally in 2022. Isoquinoline alkaloids from *Hylomecon japonica* exhibit cytotoxicity against MCF-7 cells. However, their precise molecular mechanisms, particularly with respect to apoptosis regulators, remain unclear. The present study evaluated selected isoquinoline alkaloids from *H. japonica* as potential breast cancer therapeutics through multi-computational approaches targeting Bcl-2. CPD3 displayed superior docking affinity (-7.30 kcal/mol) compared to Tamoxifen (-7.13 kcal/mol), forming one hydrogen bond and seven van der Waals interactions. Molecular dynamics simulations spanning 100 ns confirmed the complex's stability, with an average RMSD of 0.20 nm, Rg of 1.45 nm, and 1.8 hydrogen bonds for CPD3-6GL8, compared to 0.19 nm RMSD and 1.2 bonds for Tamoxifen. MMGBSA calculations revealed a binding free energy of -20.31 ± 3.12 kcal/mol for CPD3, supported by strong van der Waals contributions. ADMET prediction suggested that CPD3 has favorable pharmacokinetic properties and lower predicted toxicity than Tamoxifen, despite remaining CYP inhibition and hERG II concerns. DFT computations revealed that CPD3 possessed EHOMO of -9.2815 eV, energy gap of 9.4325 eV, and electrophilicity index of 2.2095 eV. These findings establish CPD3 as a promising Bcl-2 inhibitor, warranting further experimental validation for the management of breast cancer.

Keywords: Anti-apoptosis; Bcl-2; Breast cancer; DFT; *Hylomecon japonica*; Isoquinoline alkaloids.

INTRODUCTION

Cancer challenges in 21st century include treatment resistance, managing long-term side effects of treatments. It becomes a growing global burden due to factors like environmental influences and aging of populations. Other significant challenges involve socioeconomic and cultural factors, maintaining a humanistic approach to patient care amidst technological advancement [1, 2]. Globally, breast cancer ranks as the most common cancer diagnosis and the top cause of cancer-related deaths among women. It represents roughly 25% of new female cancer cases worldwide and led to approximately 670,000 fatalities in 2022 [3]. Breast cancer originates from the uncontrolled growth and division of breast cells, leading to the formation of tumors that can spread to other parts of the body, a process known as metastasis [4]. Numerous chemotherapeutic agents have been discovered for breast cancer treatment, and they are generally used in combination to enhance effectiveness [5]. The B-cell lymphoma 2 (Bcl-2) protein is a promising research target because it is a key regulator of the intrinsic apoptotic pathway, allowing cancer cells to evade cell death [6, 7]. In breast cancer, the overexpression of Bcl-2 is paradoxically associated with a favorable prognosis. It is strongly correlated with characteristics of less aggressive tumors, such as positive estrogen receptor and progesterone receptor status, low tumor grade, and a low proliferation rate [8]. Thus, blocking anti-apoptotic Bcl-2 proteins can restore the natural cell death process and overcome resistance to traditional chemotherapy and radiation in many malignancies.

Isoquinoline alkaloids comprise a large family of natural products derived from the isoquinoline chemical structure, which is found in many plants and is used for various medicinal purposes [9]. These compounds can induce apoptosis in various cancer cells through mechanisms such as mitochondrial dysfunction, leading to the release of cytochrome c and the activation of caspases. They also induce other cell death mechanisms, such as autophagy and cell cycle arrest, making them a focus of cancer research [10]. Previous phytochemical studies on *Hylomecon japonica* have reported the isolation of numerous isoquinoline alkaloids, some of which exhibit cytotoxic activity against the MCF-7 breast cancer cell line [11]. Nevertheless, their underlying mechanisms, especially those involving major apoptosis regulators, remain poorly understood. This study employed multiple computational techniques to investigate the anti-breast cancer potential of selected isoquinoline alkaloids from *H. japonica* and clarify their mechanism of action.

* To whom all correspondence should be sent:
Email: *hungnd@tnue.edu.vn*

MATERIALS AND METHODS

Structural preparation of selected ligands

The ligands evaluated in the present study were selected from the isoquinoline alkaloids previously isolated from *Hylomecon japonica* [11]. Among the 26 alkaloids reported in that study, 6-methoxydihydrosanguinarine (CPD1), dihydrosanguinaline (CPD2), and 10-methoxyboconoline (CPD3) were prioritized for computational analysis because of their reported cytotoxic relevance and their representativeness within the identified isoquinoline scaffold class. These alkaloids have molecular formulas of $C_{21}H_{17}NO_5$, $C_{20}H_{15}NO_4$, and $C_{23}H_{23}NO_6$, respectively, with corresponding molecular weights of 363.1107, 333.1001, and 409.1525 g/mol. Tamoxifen, possessing a molecular formula of $C_{26}H_{29}NO$ and a molecular weight of 371.2249 g/mol, was chosen as the positive control (Figure 1).

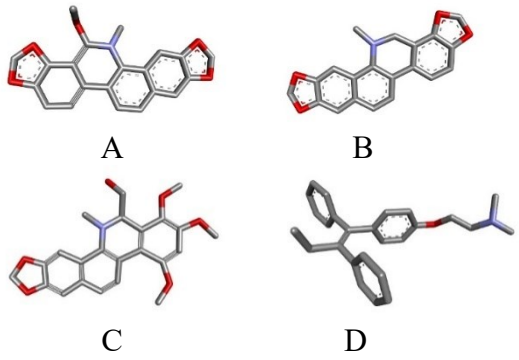

Figure 1. 3D Structures of selected ligands. (A) CPD1, (B) CPD2, (C) CPD3, (D) Tamoxifen

Molecular docking

Construction of the three-dimensional configurations for the selected ligands was performed in PDB format using Biovia Discovery Studio Visualizer, incorporating polar hydrogens, computing Gasteiger charges, and accounting for torsional bond flexibility. Acquisition of the Bcl-2 protein structure (PDB ID: 6GL8) occurred in PDB format from the RCSB Protein Data Bank [12]. Execution of ligand-protein docking utilized AutoDock Tools, employing a grid box comprising 60 points across each x, y, and z dimension at a spacing of 0.375 Å. Establishment of binding site coordinates for 6GL8 involved x = 9.866 Å, y = 0.590 Å, and z = 16.717 Å. Utilization of the Lamarckian genetic algorithm enabled the identification of conformations with minimal energy, thereby enhancing interaction stability. After docking, the highest-affinity conformation was assessed using Discovery Studio Client 2024, followed by comparison with Tamoxifen docking outcomes on the same protein to evaluate similar binding features [13].

Molecular dynamics simulation

Molecular dynamics simulations were executed to target the highest-affinity docked conformation in complex with the Bcl-2 protein (PDB ID: 6GL8) for a duration of 100 ns, using GROMACS version 2024.4 [14]. Optimization of the protein structure involved the addition of missing atoms and residues using Swiss-PdbViewer [15]. Generation of ligand force-field parameters relied on SwissParam [16]. Solvation of the protein-ligand complex occurred within a triclinic simulation box using the SPC water model supplemented with 0.15 M NaCl. Energy minimization, comprising 50,000 steps, achieved structural refinement and charge neutralization. Equilibration phases consisted of a 200 ps NVT ensemble, followed by a 200 ps NPT ensemble, both maintained at 300 K and 1 bar. Three independent production simulations, each spanning 100 ns, were performed with a 2 fs integration step, and coordinate trajectories were recorded every 10 ns. Analysis of simulation trajectories utilized Grace software to derive critical dynamical metrics, namely root mean square deviation (RMSD), root mean square fluctuation (RMSF), radius of gyration (Rg), number of hydrogen bonds (Hbonds), and solvent-accessible surface area (SASA). Evaluation of conformational stability across the simulated complexes was performed using UCSF Chimera version 1.13.3 *via* structural superposition [17].

Molecular mechanics generalized Born surface area (MMGBSA) analysis

Calculation of binding free energies for the CPD3-6GL8 and Tamoxifen-6GL8 complexes employed the gmx_MMPBSA package in conjunction with the charmm36 force field. Polar solvation energy components were derived from the generalized Born implicit solvent model, whereas non-polar terms originated from solvent-accessible surface area estimations. The extraction of data relied on molecular dynamics trajectories comprising 125 equally spaced frames, collected every 80 ps, across an 80 ns window (spanning 20 ns to 100 ns). Application of this ensemble-averaging protocol effectively delineated differences in ligand-protein interaction energetics, thereby elucidating relative binding affinities and complex stability throughout the simulation period [18].

Assay protocol for ADMET prediction

A concise evaluation of ADMET characteristics, encompassing absorption, distribution, metabolism,

excretion, and toxicity, constitutes a fundamental step in early drug discovery because pharmacokinetic liabilities and potential safety risks can be recognized before advanced development stages. Such analysis contributes to lower attrition in subsequent phases and supports prioritization of molecules with favorable therapeutic prospects. For the present analysis, ADMET profiles of CPD3 and Tamoxifen were estimated with the pkCSM platform, a computational framework based on graph-derived molecular descriptors. Use of this platform enabled the prediction of major pharmacokinetic and toxicological parameters and allowed a systematic comparison of developability-related properties for the compounds examined.

Quantum chemistry computation using the Density Functional Theory (DFT) method

Optimization of molecular geometries for CPD3 and Tamoxifen utilized the ORCA quantum chemistry package version 6.1.0. Generation of initial coordinates occurred in Avogadro, whereas subsequent visualization of molecular orbitals and associated analyses employed IboView version 20211019 [19-21]. All density functional theory calculations employed the B3LYP functional in conjunction with the 6-31G(d,p) basis set to generate accurate electronic wave functions. From the fully optimized structures, extraction of key quantum-chemical descriptors proceeded, comprising energies of the highest occupied molecular orbital (HOMO) and the lowest unoccupied molecular orbital (LUMO), the HOMO-LUMO energy gap (ΔE), chemical potential (μ), electronegativity (χ), global hardness (η), softness (σ), and electrophilicity index (ω). Determination of these reactivity parameters was approximately based on Kohn-Sham HOMO/LUMO energies within conceptual DFT to characterize the electronic properties and chemical behavior of the investigated compounds [22, 23].

RESULTS AND DISCUSSION

Molecular docking analysis

Molecular docking is a computational technique in natural product research that predicts how a natural compound binds to a protein target, aiding in the screening of potential drugs and in understanding their mechanisms. This process allows researchers to virtually screen vast libraries of natural compounds to identify promising candidates for experimental validation, saving time and resources compared to traditional laboratory methods [24, 25]. Examination of docking affinities and intermolecular interactions was conducted for three selected ligands bound to the Bcl-2 protein (PDB ID: 6GL8), using Tamoxifen as a reference. Table 1 presents the residues that constitute the binding pocket and their contributions to the interaction profile between these ligands and 6GL8, focusing on non-covalent forces, including hydrogen bonds, van der Waals forces, and hydrophobic interactions between the protein and the ligands. Ligands CPD1-CPD3 demonstrated diverse engagement patterns with Bcl-2, a pivotal modulator of apoptotic pathways in oncogenic processes. CPD1 established 10 interactions in total, incorporating 2 hydrogen bonds (Gly145, Arg146), 4 van der Waals forces (Phe104, Asp111, Phe112, Leu137), and 4 hydrophobic interactions (Tyr108, Met115, Arg146, Ala149) (Figure 2A). Participating binding site residues comprised Phe104, Tyr108, Asp111, Phe112, Leu137, Gly145, Arg146, and Ala149, resulting in a binding energy of -6.65 kcal/mol for the CPD1-6GL8 complex. CPD2 registered 9 interactions: no hydrogen bonds, 6 van der Waals forces (Phe104, Tyr108, Asp111, Phe112, Gln118, Phe153), and 3 hydrophobic interactions (Met115, Leu119, Val133). Pocket residues involved Phe104, Tyr108, Asp111, Phe112, Gln118, and Phe153, achieving a binding energy of -6.38 kcal/mol, indicative of moderate stabilization.

Table 1. Interactions between docked ligands and protein 6GL8.

Docked ligands	Binding energy (kcal/mol)	Hydrogen bond interaction	Van der Waals interaction	Hydrophobic interaction
CPD1	-6.65	Gly145, Arg146	Phe104, Asp111, Phe112, Leu137	Tyr108, Met115, Arg146, Ala149
CPD2	-6.38	-	Phe104, Tyr108, Asp111, Phe112, Gln118, Phe153	Met115, Leu119, Val133
CPD3	-7.30	Ala149	Phe104, Asp111, Phe112, Gln118, Leu137, Glu152, Phe153	Tyr108, Met115, Leu119, Val133
Tamoxifen	-7.13	Glu136	Phe104, Tyr108, Glu114, Gln118, Thr132, Val133, Leu137, Glu152, Phe153	Asp111, Phe112, Met115, Ala149

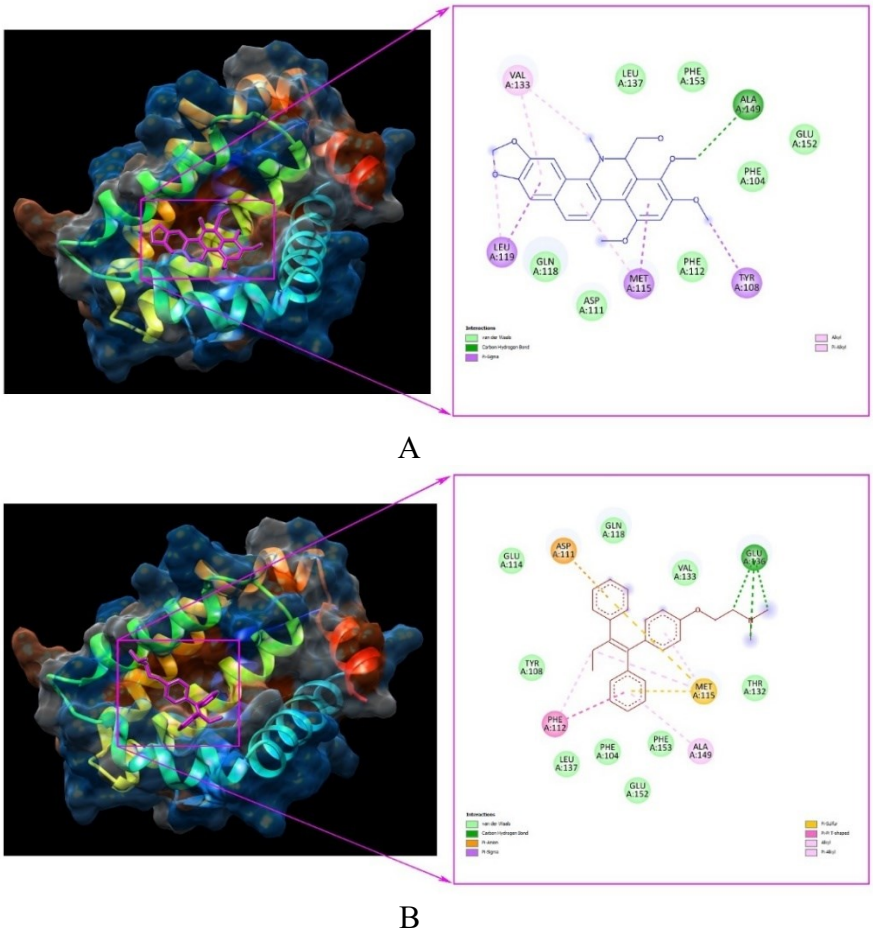

Figure 2. Molecular docking model and 2D diagram of CPD3 (A) and Tamoxifen (B) interaction with 6GL8 protein

CPD3 distinguished itself with 12 interactions: 1 hydrogen bond (Ala149), 7 van der Waals forces (Phe104, Asp111, Phe112, Gln118, Leu137, Glu152, Phe153), and 4 hydrophobic interactions (Tyr108, Met115, Leu119, Val133) (Figure 2A). Residues at the site included Phe104, Tyr108, Asp111, Phe112, Gln118, Leu137, Ala149, and Phe153, achieving the highest binding energy of -7.30 kcal/mol, indicating a robust attachment. For comparison, Tamoxifen generated 14 interactions, featuring 1 hydrogen bond (Glu136), 9 van der Waals forces (Phe104, Tyr108, Glu114, Gln118, Thr132, Val133, Leu137, Glu152, Phe153), and 4 hydrophobic interactions (Asp111, Phe112, Met115, Ala149) (Figure 2B). Binding site residues encompassed Phe104, Tyr108, Asp111, Phe112, Gln118, Leu137, Ala149, and Phe153, with an energy value of -7.13 kcal/mol. Although Tamoxifen displayed a reliable association, its comparatively less negative energy and interaction composition implied a diminished overall affinity relative to CPD3, which surpassed it in binding strength. These docking findings underscore an array of non-covalent modalities that underpin complex integrity, ranging from hydrogen bonds that enable precise atomic alignment with electronegative atoms to hydrophobic interactions that reduce aqueous exposure, thereby promoting condensed structures [26]. Van der Waals contributions provided nuanced enhancement *via* short-range interactions, augmenting the ensemble to optimize association kinetics [27]. Greater negativity in binding energy, meaning a more negative value, typically correlates with enhanced complex durability and stronger ligand sequestration at the receptor site [28].

Owing to its exceptional docking characteristics against 6GL8, characterized by an energy of -7.30 kcal/mol and 12 interactions, CPD3 surfaced as the prime contender for further molecular dynamics explorations. This superiority relative to counterparts, including CPD2 (-6.38 kcal/mol) and Tamoxifen (-7.13 kcal/mol), designates CPD3 for comprehensive evaluation of structural dynamics, energetic profiles, and amino acid involvements across temporal scales, employing Tamoxifen as a comparative reference in probing apoptosis regulation for therapeutic interventions in breast cancer.

Molecular dynamics simulation

Molecular dynamics simulation and docking are computational techniques used together in natural product research to identify and validate potential new drug candidates from natural sources. The combination of molecular docking and molecular dynamics simulation improves the accuracy and efficiency of drug discovery by helping to rank potential compounds before experimental testing [29]. Therefore, the evaluation systematically investigated RMSD, RMSF, Rg, Hbonds, and SASA metrics to determine the stability, flexibility, and solvent exposure of the CPD3-6GL8 and Tamoxifen-6GL8 complexes throughout the simulation. Consequently, the total energy and potential energy values for the CPD3-6GL8 complex were found to be -227,476 kJ/mol and -282,483 kJ/mol, respectively. For the Tamoxifen-6GL8 complex, the total energy and potential energy values were measured at -227,598 kJ/mol and -282,593 kJ/mol, respectively. The simulation system maintained equilibrium at a temperature of 300 K.

Elevated RMSD values signify substantial deviations from the baseline conformation, whereas diminished values denote preserved structural fidelity. Throughout the 100 ns trajectory, RMSD profiles for the CPD3-6GL8 and Tamoxifen-6GL8 assemblies exhibited discernible variations (Figure 3A). The CPD3-6GL8 assembly exhibited RMSD magnitudes predominantly ranging from 0.15 to 0.28 nm, with an approximate mean of 0.20 nm, indicating substantial structural stability and firm ligand anchorage within the 6GL8 pocket. Conversely, the Tamoxifen-6GL8 assembly exhibited oscillations between 0.15 and 0.25 nm, averaging approximately 0.19 nm, indicating moderate flexibility despite overall conformational resilience. Such disparities underscore a marginally enhanced equilibrium for the CPD3-6GL8 assembly compared to the Tamoxifen-6GL8 assembly, potentially attributable to optimized intermolecular interactions at the binding interface. In aggregate, the RMSD metrics indicate superior retention of the native architecture in the CPD3-6GL8 assembly compared with the Tamoxifen-6GL8 assembly over the simulation duration. Figure 3B displays RMSF profiles for the CPD3-6GL8 and Tamoxifen-6GL8 complexes over residues from approximately 1 to 2000, with magnitudes generally confined to the 0.05 to 0.25 nm interval. In the CPD3-6GL8 complex, deviations hover steadily around 0.1 nm throughout most of the polypeptide chain, indicating constrained flexibility and enhanced structural rigidity, likely due to stabilizing interactions at loci such as Phe104, Leu137, and Phe153.

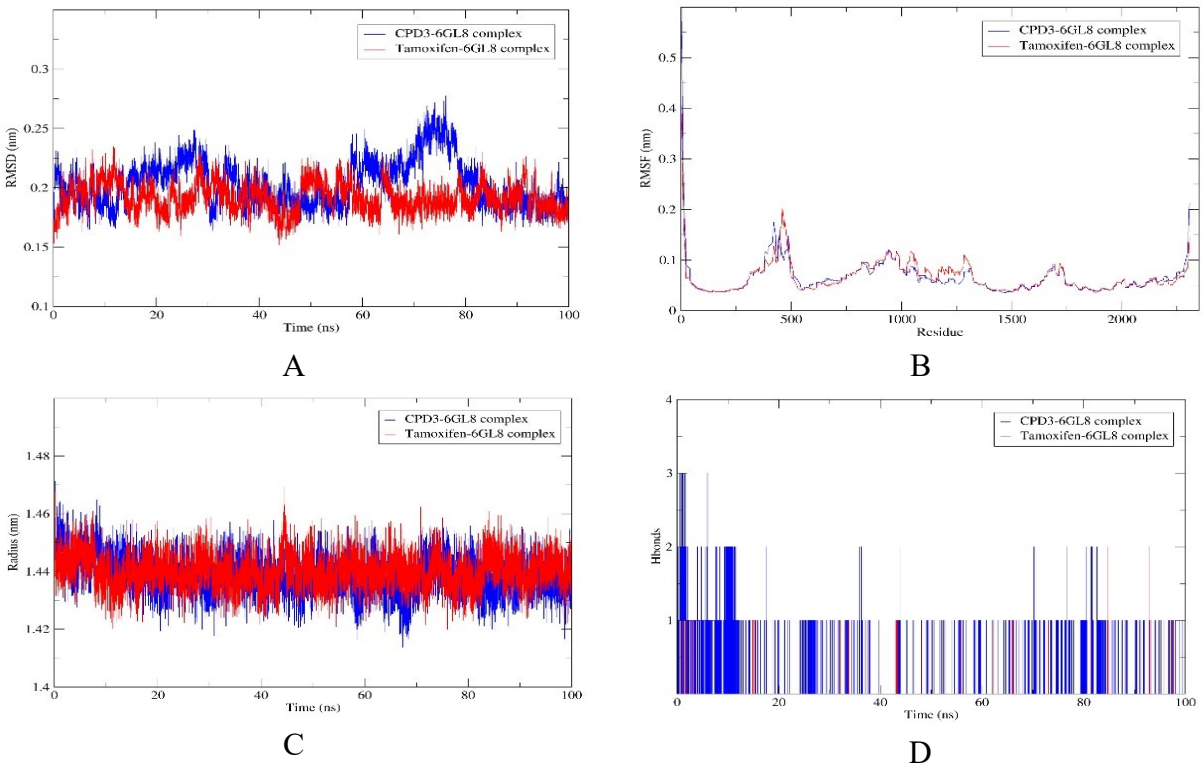

Figure 3. Results of MD simulation for the bindings of CPD3 (blue) and Tamoxifen (red) with 6GL8 protein. (A) RMSD, (B) RMSF, (C) Rg, (D) Hbonds, (E) SASA

The Tamoxifen-6GL8 complex exhibits an analogous pattern characterized by an average deviation of approximately 0.1 nm, accompanied by modest oscillations and correspondences, and indicating equivalent levels of conformational restraint. This congruence across both assemblies highlights the capacity of ligands to stabilize protein structure, thereby facilitating sustained interactions in functional domains. Figure 3C illustrates Rg trajectories for CPD3-6GL8 and Tamoxifen-6GL8 complexes throughout 100 ns, with both profiles exhibiting consistent fluctuations between 1.42 and 1.48 nm and an estimated average of 1.45 nm, signifying preservation of a tightly organized and compact configuration in the 6GL8 protein under ligand-bound conditions during the entire simulation period. Throughout the 100 ns duration, counts of hydrogen bonds within the CPD3-6GL8 complex varied between 1 and 3, in contrast to 0 and 2 bonds observed in the Tamoxifen-6GL8 complex (Figure 3D). These consistent associations indicate firm integration into the 6GL8 pocket for both configurations, although the CPD3-6GL8 complex generally maintained an average close to 1.8, surpassing the approximate 1.2 observed for Tamoxifen-6GL8. Such variation underscores CPD3's enhanced capacity to establish persistent connections with the protein. Evaluation of SASA profiles was performed for the CPD3-6GL8 and Tamoxifen-6GL8 complexes to assess changes in solvent exposure. Across the 100 ns timeframe, both demonstrated persistent variations, ranging roughly from 80 to 92 nm² with an estimated mean of 86 nm². These behaviors suggest minor adjustments in protein-solvent interactions in the presence of ligands, which may influence binding longevity. Equivalent extents and central values across the complexes denote equilibrated solvent interaction, signifying robust persistence at the 6GL8 binding domain despite differences in ligand attributes. A comprehensive appraisal of dynamical parameters elucidates the conformational equilibrium and associative characteristics in the CPD3-6GL8 and Tamoxifen-6GL8 complexes, highlighting the role of the 6GL8 protein in ligand coordination. Results indicate that the CPD3-6GL8 complex configuration exhibits slightly greater resilience compared to the Tamoxifen-6GL8 equivalent within the 6GL8 framework, positioning CPD3 as a promising candidate for further investigation. These observations validate CPD3's ability to maintain strong, lasting interactions with the 6GL8 protein.

Free binding energy (MMGBSA) analysis

Molecular mechanics with generalized Born surface area (MMGBSA) is a computational method used in natural product research to estimate the binding free energy of molecules and identify potential drug candidates. It combines molecular mechanics force fields with continuum solvation models, including generalized Born for polar solvents and surface area for non-polar solvation, to provide a fast and accurate method for predicting the binding affinity of a natural product or its derivative to a biological target. This approach can be complemented by techniques such as virtual screening and molecular dynamics simulations. This technique is widely used to understand the thermodynamics of a protein-ligand complex and identify key interactions that contribute to stable binding [38]. Estimation of binding free energies for the complexes employed the MMGBSA methodology with gmx_MMPBSA and the CHARMM36 force field. Selection of frames from molecular dynamics trajectories spanning 80 ns facilitated this computation. For both instances, calculation of binding free energy (ΔG_bind) adhered to ΔG_bind = G_complex - (G_receptor + G_ligand), where G_receptor denotes the energy of the free receptor, and G_ligand represents the energy of the unbound ligand. Alternatively, expression as ΔG_bind = ΔH - TΔS was observed, with ΔH encompassing enthalpic contributions and -TΔS capturing entropic penalties during association. Exclusion of entropy contributions provided a relative energy indicator suitable for affinity comparisons across similar systems. The focus of this evaluation was the 80 ns segment, with 125 frames extracted at 80 ps intervals (ranging from 20 ns to 100 ns). The implementation of this protocol yielded averaged energies that captured the temporal progression of associations, providing insights into compound potency and resilience in modeled physiological settings. The results of MMGBSA computations for the complexes are shown in Table 2. Alignment of these derived binding energies with simulation data manifests, displaying Tamoxifen-6GL8's marginally advantageous value (-22.34 ± 2.87 kcal/mol) relative to CPD3-6GL8 (-20.31 ± 3.12 kcal/mol), consistent with its somewhat enhanced overall adherence. Nevertheless, CPD3-6GL8 exhibits slightly diminished structural variability, as evidenced by its slightly higher average RMSD (approximately 0.20 nm *versus* 0.19 nm), indicating comparable positioning but a higher prevalence of hydrogen bonds, suggesting more extensive interfacial connectivity.

Table 2. Free energy of binding obtained using MMGBSA calculations.

Energy component	Average (kcal/mol)		Standard deviation	
	CPD3-6GL8	Tamoxifen-6GL8	CPD3-6GL8	Tamoxifen-6GL8
ΔVDWAΔALS	-32.15	-36.85	3.57	3.16
ΔEEL	-11.4	0.77	4.34	2.85
ΔEGB	27.53	18.82	4.75	2.77
ΔESURF	-4.29	-5.08	0.47	0.45
ΔGGAS	-43.55	-36.08	6.68	3.64
ΔGSOLV	23.24	13.73	4.43	2.75
ΔTOTAL	-20.31	-22.34	3.12	2.87

Concurrently, equivalent RMSF (around 0.1 nm), Rg (approximately 1.45 nm average), and SASA (near 86 nm² mean) distributions across both underscore Tamoxifen's edge in affinity likely arise from specific enthalpic factors, including van der Waals (-36.85 kcal/mol) and solvation terms (ΔGSOLV 13.73 kcal/mol), surpassing CPD3's (-32.15 and 23.24 kcal/mol, respectively). In summary, these indicators reveal Tamoxifen's modestly elevated potential for forming a stable complex with the 6GL8 protein under the assessed circumstances.

ADMET prediction analysis

ADMET profiling suggested that CPD3 combines favorable oral absorption with a distribution pattern less indicative of central nervous system exposure than tamoxifen, and it shows fewer mutagenicity and cardiotoxicity alerts in the current prediction panel. Early ADMET evaluation is valuable because permeability, transport, metabolism, and toxicity often influence developability as strongly as target affinity [30]. The ADMET prediction results are shown in Table 3. Regarding absorption, CPD3 showed slightly better predicted aqueous solubility than Tamoxifen (log S -5.136 *vs*. -5.929), while both compounds maintained high intestinal absorption (98.629% and 96.885%, respectively). Caco-2 permeability was favorable for both ligands, with values above the usual high-permeability threshold (1.242 for CPD3; 1.065 for Tamoxifen). Skin permeability was nearly identical, suggesting similarly limited transdermal passage. A notable difference was that CPD3 was predicted not to be a P-glycoprotein substrate, whereas Tamoxifen was, although both were predicted to inhibit P-glycoprotein I and II. This may indicate reduced efflux susceptibility for CPD3, but possible transporter-related interaction risks still require experimental confirmation [31]. Distribution parameters differentiated the compounds more clearly. CPD3 showed a low predicted steady-state volume of distribution (log VDss = -0.493), whereas Tamoxifen had a much higher value (0.830), suggesting broader tissue distribution for the reference drug [32]. Both compounds had low and similar unbound fractions in plasma (Fu 0.097 for CPD3; 0.093 for Tamoxifen), consistent with extensive plasma protein binding. Brain exposure descriptors also favored CPD3 as a more peripheral compound: log BB/log PS values were -0.342/-3.100 for CPD3 *versus* 1.329/-1.473 for Tamoxifen, indicating substantially lower BBB penetration and CNS access for CPD3.

The Boiled-egg model supported this trend. CPD3 fell in the white region but outside the yellow yolk, consistent with high gastrointestinal absorption and limited passive BBB permeation, whereas Tamoxifen was located in the yolk region, indicating greater passive brain entry (Figure 4). However, because the plot showed both compounds as P-glycoprotein substrates despite the tabulated output identifying only Tamoxifen as such, transporter interpretation should rely on the table, while the Boiled-egg plot is best used here to assess GI absorption and BBB region placement [33].

Table 3. Predicted ADMET properties of CPD3 and Tamoxifen

ADMET properties	Unit	CPD3	Tamoxifen
Water solubility	(Log mol/L)	-5.136	-5.929
CaCo2 permeability	(Log Papp in 10-6 cm/s)	1.242	1.065
Intestinal absorption (human)	(% Absorbed)	98.629	96.885
Skin permeability	(Log Kp)	-2.736	-2.737
P-glycoprotein substrate	Yes/No	No	Yes
P-glycoprotein I inhibitor	Yes/No	Yes	Yes
P-glycoprotein II inhibitor	Yes/No	Yes	Yes
VDss	(Log L/kg)	-0.493	0.830
Fraction unbound (human)	(Fu)	0.097	0.093
BBB permeability	(Log BB)	-0.342	1.329
CNS permeability	(Log PS)	-3.100	-1.473
CYP2D6 substrate	Yes/No	No	No
CYP3A4 substrate	Yes/No	Yes	Yes
CYP1A2 inhibitor	Yes/No	No	Yes
CYP2C19 inhibitor	Yes/No	Yes	No
CYP2C9 inhibitor	Yes/No	Yes	No
CYP2D6 inhibitor	Yes/No	No	Yes
CYP3A4 inhibitor	Yes/No	Yes	No
Total clearance	(Log ml/min/kg)	0.456	0.556
Renal OCT2 substrate	Yes/No	No	No
AMES toxicity	Yes/No	No	Yes
Max. tolerated dose (human)	(Log mg/kg/day)	0.257	0.313
hERG I inhibitor	Yes/No	No	Yes
hERG II inhibitor	Yes/No	Yes	Yes
Oral rat acute toxicity (LD50)	(mol/kg)	2.622	2.285
Oral rat chronic toxicity (LOAEL)	(Log mg/kg_bw/day)	1.035	0.41
Hepatotoxicity	Yes/No	No	No
Skin sensation	Yes/No	No	No
Tetrahymena pyriformis toxicity	(Log µg/L)	0.288	0.316
Minnow toxicity	(Log mM)	-0.892	0.600

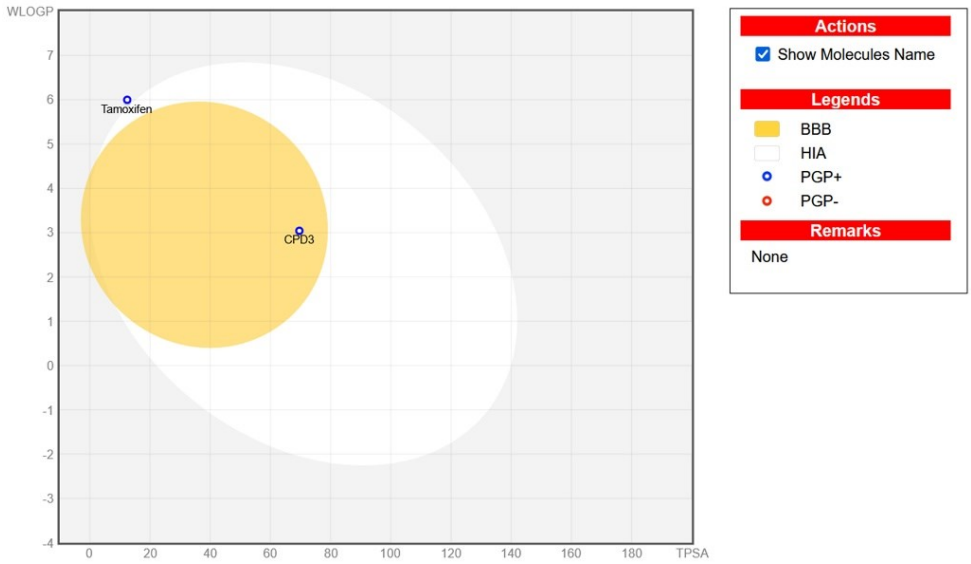

Figure 4. Boiled-egg plot of the selected compounds, generated from Swiss ADME

Metabolically, both compounds were predicted to be CYP3A4 substrates rather than CYP2D6 substrates, suggesting a role for CYP3A4 in clearance. Their inhibition profiles differed. CPD3 was predicted to inhibit CYP2C19, CYP2C9, and CYP3A4, but not CYP1A2 or CYP2D6 [34]. Tamoxifen showed the opposite pattern across several isoforms, inhibiting CYP1A2 and CYP2D6 but not CYP2C19, CYP2C9, or CYP3A4. These results suggest distinct drug-drug interaction risks rather than a clearly safer metabolic profile for either compound.

Excretion differences were modest. Total clearance was slightly lower for CPD3 than for Tamoxifen (0.456 vs. 0.556 log ml/min/kg), suggesting somewhat slower elimination. Neither compound was predicted to be a renal OCT2 substrate [35]. Together with the low unbound fraction, this suggests CPD3 may maintain systemic exposure while distributing less extensively into tissues than Tamoxifen.

The toxicity panel favored CPD3 in several important endpoints. CPD3 was predicted to be Ames-negative, whereas Tamoxifen was Ames-positive, indicating lower mutagenic concern. CPD3 was also negative for hERG I inhibition, while tamoxifen carried a positive hERG I alert; both compounds remained positive for hERG II inhibition. Both were predicted to be non-hepatotoxic and non-sensitizing to skin. Thus, CPD3 appears to have a more favorable early safety profile, although electrophysiological follow-up remains necessary due to the retained hERG II signal [36]. Quantitative toxicity endpoints provided additional detail. Both compounds showed low predicted maximum tolerated doses in humans, below the common threshold. CPD3 also showed slightly better acute and chronic oral toxicity profiles in rats, with a higher LD50 and LOAEL than Tamoxifen [37]. *Tetrahymena pyriformis* toxicity values were comparable for both compounds, whereas Minnow toxicity was less favorable for CPD3, indicating a stronger predicted aquatic toxicity signal.

Overall, CPD3 demonstrated a pharmacokinetic and safety profile supportive of further development as a breast cancer lead. It combined excellent oral absorption, high Caco-2 permeability, strong predicted intestinal uptake, limited BBB penetration, lack of Ames toxicity, and absence of an hERG I alert. However, low solubility, strong plasma binding, CYP inhibition liabilities, persistent hERG II risk, and unfavorable Minnow toxicity remain relevant concerns. Taken together, the ADMET and BOILED-Egg results support CPD3 as a promising compound with improved early safety features over Tamoxifen, while still requiring experimental validation of transporter, metabolic, cardiac, and ecological liabilities.

Quantum chemistry computation using the DFT method

DFT is a powerful quantum-mechanical method used in natural product research to computationally model and predict the electronic structure and properties of molecules. It offers a balance between accuracy and computational cost, making it ideal for studying complex natural products, and is used to investigate properties like chemical reactivity, host-guest interactions, and solubilization mechanisms [39]. Quantum chemistry computations are frequently performed after molecular docking and dynamics simulations to achieve high accuracy in validating and refining the results of classical mechanics methods. In this study, DFT calculations were employed to examine the electronic properties and potential reactivity of CPD3 and Tamoxifen, drawing from the specified descriptors. The derived values encompass energies of the highest occupied molecular orbitals (EHOMO), lowest unoccupied molecular orbitals (ELUMO), energy gap (ΔE), chemical potential (μ), electronegativity (χ), hardness (η), softness (σ), and electrophilicity index (ω). These EHOMO and ELUMO energies offer key insights into electron arrangements, molecular stability, and interaction tendencies within the compounds. EHOMO gauges the ease of electron release, while ELUMO assesses the ability to accept electrons. For CPD3, EHOMO stands at -9.2815 eV, which is lower than Tamoxifen's -8.2093 eV, suggesting that CPD3 is less prone to electron donation and exhibits greater stability against oxidation (Figure 5). Conversely, CPD3's ELUMO of 0.1510 eV is notably below Tamoxifen's 3.2074 eV, indicating CPD3's enhanced aptitude for electron capture. The energy gap (ΔE), calculated as ELUMO less EHOMO, reflects overall durability and chemical responsiveness; smaller gaps correlate with elevated activity and adaptability, whereas larger ones suggest enhanced resilience (Table 4). CPD3's ΔE of 9.4325 eV is smaller compared to Tamoxifen's ΔE of 11.4167 eV, implying that CPD3 has comparatively lower endurance but increased potential for reactions. The ionization potential (IP), defined as -EHOMO, is the energy required to detach an electron; higher values indicate greater oxidation resistance.

Table 4. Quantum descriptors of CPD3 and Tamoxifen.

Molecule	EHOMO (eV)	ELUMO (eV)	ΔE (eV)	μ (eV)	χ (eV)	η (eV)	σ (eV^{-1})	ω (eV)
CPD3	-9.2815	0.1510	9.4325	-4.5653	4.5653	4.7163	0.2120	2.2095
Tamoxifen	-8.2093	3.2074	11.4167	-2.5010	2.5010	5.7084	0.1752	0.5479

EHOMO (eV): highest occupied molecular orbitals; ELUMO (eV): lowest unoccupied molecular orbitals; ΔE (eV): energy gap; μ (eV): chemical potential; χ (eV): electronegativity; η (eV): hardness; σ (eV^{-1}): softness; ω (eV): electrophilicity index.

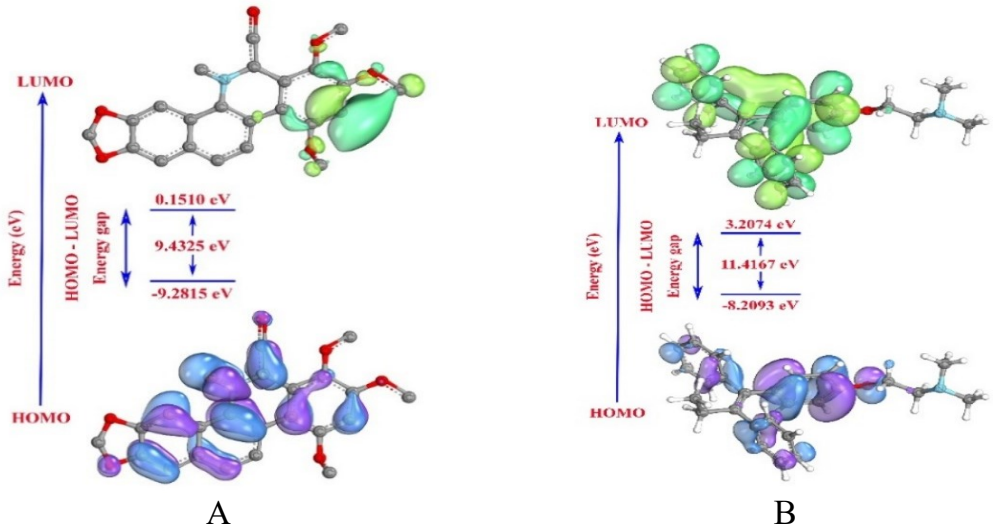

Figure 5. HOMO and LUMO surface diagrams of CPD3 (A) and Tamoxifen (B)

Electron affinity (EA), as measured by -ELUMO, quantifies the ease of electron incorporation; higher values indicate greater electron affinity. Thus, CPD3 shows an IP of 9.2815 eV and EA of -0.1510 eV, *versus* Tamoxifen's IP of 8.2093 eV and EA of -3.2074 eV, highlighting CPD3's superior resistance to electron loss alongside modestly improved electron attraction. Tamoxifen, in contrast, is more amenable to electron release but exhibits weaker electron affinity. Hardness (η), obtained from ΔE/2, evaluates resistance to shifts in electron density, and softness (σ), as 1/η, indicates flexibility in chemical engagements. CPD3 registers hardness of 4.7163 eV and softness of 0.2120 eV^{-1}, compared to Tamoxifen's hardness of 5.7084 eV and softness of 0.1752 eV^{-1}, indicating that CPD3 is more accommodating to electronic adjustments (Figure 4). Electronegativity (χ), determined by (IP + EA)/2, quantifies the pull on electrons in bonds. CPD3's χ at 4.5653 eV exceeds Tamoxifen's 2.5010 eV, revealing CPD3's greater affinity for electrons in shared pairs. Chemical potential (μ), equivalent to -χ, directs the flow of electrons; lower (more negative) values promote intake. Accordingly, CPD3's μ of -4.5653 eV is more negative than Tamoxifen's -2.5010 eV, underscoring CPD3's stronger drive toward electron accumulation. Lastly, the electrophilicity index (ω), defined as $\mu^2/(2\eta)$, quantifies the tendency to attract electrons, with larger values indicating greater electrophilicity. CPD3's ω of 2.2095 eV substantially outpaces Tamoxifen's 0.5479 eV, proposing CPD3 may interact more dynamically as an electrophile with nearby species.

CONCLUSION

This study investigated isoquinoline alkaloids from *H. japonica* as potential breast cancer inhibitors, with a focus on the Bcl-2 protein (6GL8), a key regulator of cell death. CPD3 exhibited stronger docking performance (-7.30 kcal/mol) than Tamoxifen (-7.13 kcal/mol), with 12 interactions, including 1 hydrogen bond and 7 van der Waals interactions. Over 100 ns simulations, the CPD3-6GL8 complex demonstrated solid stability, with a mean RMSD of around 0.20 nm, a radius of gyration (Rg) of approximately 1.45 nm, and approximately 1.8 hydrogen bonds, compared to Tamoxifen's 0.19 nm RMSD and about 1.2 bonds. MMGBSA results indicated stronger binding for CPD3 (-20.31 ± 3.12 kcal/mol) than for Tamoxifen (-22.34 ± 2.87 kcal/mol), supported by van der Waals terms (-32.15 kcal/mol) and solvation (ΔGSOLV 23.24 kcal/mol). ADMET prediction suggested that CPD3 combines excellent intestinal absorption, favorable permeability, limited BBB and CNS penetration, absence of AMES toxicity, and no hERG I

inhibition, indicating more favorable early safety and pharmacokinetic profile than Tamoxifen, although potential CYP-mediated drug-drug interactions, hERG II liability, and ecological toxicity concerns remain. DFT analysis revealed CPD3's electronic properties, with EHOMO at -9.2815 eV, ΔE of 9.4325 eV, and ω of 2.2095 eV, compared to Tamoxifen's (-8.2093 eV, 11.4167 eV, and 0.5479 eV). Overall, these outcomes highlight CPD3 as a viable option for breast cancer therapy, meriting additional refinement and testing in cancer research.

REFERENCES

1. G. Colonna, *Cancers*, **17**, 2102 (2025).
2. M. J. Thun, J. O. DeLancey, M. M. Center, A. Jemal, E. M. Ward, *Carcinogenesis*, **31**, 100 (2010).
3. F. Bray, M. Laversanne, H. Sung, J. Ferlay, R. L. Siegel, I. Soerjomataram, A. Jemal, *CA. Cancer J. Clin.*, **74**, 229 (2024).
4. S. D. Nathanson, M. Detmar, T. P. Padera, L. R. Yates, D. R. Welch, T. C. Beadnell, A. D. Scheid, E. D. Wrenn, K. Cheung, *Clin. Exp. Metastasis*, **39**, 117 (2022).
5. E. Carvalho, S. Canberk, F. Schmitt, N. Vale, *Cancers*, **17**, 1102 (2025).
6. A. Kawiak, A. Kostecka, *Cancers*, **14**, 279 (2022).
7. S. Qian, Z. Wei, W. Yang, J. Huang, Y. Yang, J. Wang, *Front. Oncol.*, **12**, 985363 (2022).
8. H. Azmat, J. Faridi, H. M. Habib, U. J. Bugti, A. K. Sheikh, S. K. Riaz, *J. Cancer Res. Ther.*, **18**, S313 (2022).
9. A. Y. Khan, G. Suresh Kumar, *Biophys. Rev.*, **7**, 407 (2015).
10. X. Yang, T. Bu, Y. Ma, X. Yu, Z. Gong, J. Wang, X. Liu, J. Jenis, H. Hu, X. Miao, X. Shang, *Ind. Crops Prod.*, **234**, 121591 (2025).
11. Z. Cao, S. Zhu, Z. Xue, F. Zhang, L. Zhang, Y. Zhang, Y. Guo, G. Zhan, X. Zhang, Z. Guo, *Phytochemistry*, **202**, 113321 (2022).
12. J. B. Murray *et al.*, *ACS Omega*, **4**, 8892 (2019).
13. H. D. Nguyen, *Not. Sci. Biol.*, **17**, 12642 (2025).
14. D. Van Der Spoel, E. Lindahl, B. Hess, G. Groenhof, A. E. Mark, H. J. C. Berendsen, *J. Comput. Chem.*, **26**, 1701 (2005).
15. N. Guex, M. C. Peitsch, *Electrophoresis*, **18**, 2714 (1997).
16. V. Zoete, M. A. Cuendet, A. Grosdidier, O. Michielin, *J. Comput. Chem.*, **32**, 2359 (2011).
17. E. F. Pettersen, T. D. Goddard, C. C. Huang, G. S. Couch, D. M. Greenblatt, E. C. Meng, T. E. Ferrin, *J. Comput. Chem.*, **25**, 1605 (2004).
18. H. D. Nguyen, *Phys. Chem. Res.*, **13**, 783 (2025).
19. F. Neese, *WIREs Comput. Mol. Sci.*, **15**, e70019 (2025).
20. G. Knizia, J. E. M. N. Klein, *Angew. Chemie Int. Ed.*, **54**, 5518 (2015).
21. M. D. Hanwell, D. E. Curtis, D. C. Lonie, T. Vandermeersch, E. Zurek, G. R. Hutchison, *J. Cheminform.*, **4**, 17 (2012).
22. J. Luo, Z. Q. Xue, W. M. Liu, J. L. Wu, Z. Q. Yang, *J. Phys. Chem. A*, **110**, 12005 (2006).
23. R. Das, J.L. Vigneresse, P. K. Chattaraj, *Int. J. Quantum Chem.*, **114**, 1421 (2014).
24. I. Asiamah, S. A. Obiri, W. Tamekloe, F. A. Armah, L. S. Borquaye, *Sci. African*, **20**, e01593 (2023).
25. P. C. Agu, C. A. Afiukwa, O. U. Orji, E. M. Ezeh, I. H. Ofoke, C. O. Ogbu, E. I. Ugwuja, P. M. Aja, *Sci. Rep.*, **13**, 13398 (2023).
26. R. Patil, S. Das, A. Stanley, L. Yadav, A. Sudhakar, A. K. Varma, *PLoS One*, **5**, e12029 (2010).
27. G. Bitencourt-Ferreira, M. Veit-Acosta, W. F. de Azevedo, Van der Waals potential in protein complexes (Docking screens for drug discovery), Springer, New York, 2019.
28. N. T. Issa, E. V Badiavas, S. Schürer, *J. Invest. Dermatol.*, **139**, 2400 (2019).
29. A. R. Alanzi, B. A. Alhaidhal, R. M. Aloatibi, *Sci. Rep.*, **15**, 16385 (2025).
30. D. E. Pires, T. L. Blundell, D. B. Ascher, *J. Med. Chem.*, **58**, 4066 (2015).
31. G. Falcón-Cano, C. Molina, M. Á. Cabrera-Pérez, *Pharmaceutics*, **14**, 1998 (2022).
32. M. Gupta, J. Feng, G. Bhisetti, *Molecules*, **29**, 1264 (2024).
33. R. Kato, W. Zeng, V. B. Siramshetty, J. Williams, M. Kabir, N. Hagen, E. C. Padilha, A. Q. Wang, E. A. Mathé, X. Xu, P. Shah, *Front. Pharmacol.*, **14**, 1291246 (2023).
34. J. Lee, J. L. Beers, R. M. Geffert, K. D. Jackson, *Biomolecules*, **14**, 99 (2024).
35. K. Korzekwa, S. Nagar, *Drug Metab. Dispos.*, **51**, 532 (2023).
36. P. Delre, G. J. Lavado, G. Lamanna, M. Saviano, A. Roncaglioni, E. Benfenati, G. F. Mangiatordi, D. Gadaleta, *Front. Pharmacol.*, **13**, 951083 (2022).
37. A. L. Karmaus, K. Mansouri, K. T. To, B. Blake, J. Fitzpatrick, J. Strickland, G. Patlewicz, D. Allen, W. Casey, N. Kleinstreuer, *Toxicol. Sci.*, **188**, 34 (2022).
38. M. E. Valdés-Tresanco, M. S. Valdés-Tresanco, E. Moreno, P. A. Valiente, *J. Phys. Chem. B*, **127**, 944 (2023).
39. H. Guan, H. Sun, X. Zhao, *Int. J. Mol. Sci.*, **26**, (2025).